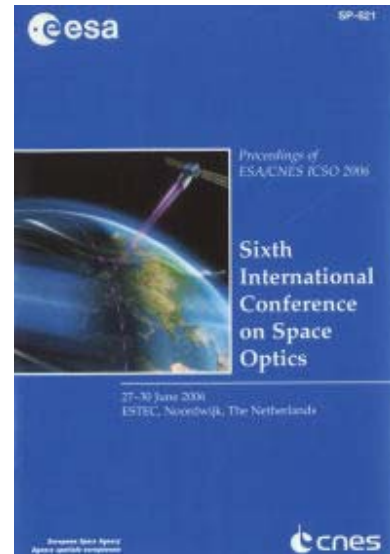


International Conference on Space Optics—ICSO 2006

Noordwijk, Netherlands

27–30 June 2006

Edited by Errico Armandillo, Josiane Costeraste, and Nikos Karafolas



I.C.E.: a transportable atomic inertial sensor for test in microgravity

R. A. Nyman, G. Varoquaux, J.-F. Clement, P. Bouyer, et al.



I.C.E.: A TRANSPORTABLE ATOMIC INERTIAL SENSOR FOR TEST IN MICROGRAVITY

R. A. Nyman¹, G. Varoquaux¹, J.-F. Clément¹, P. Bouyer¹, G. Santarelli², F. Pereira Dos Santos², A. Clairon², A. Landragin², D. Chambon³, F. Lienhart³, S. Boussem³, and A. Bresson³

¹Laboratoire Charles Fabry de l'Institut d'Optique, Centre National de la Recherche Scientifique et Université Paris Sud 11, Bât. 503, Campus Universitaire d'Orsay, 91403 Orsay Cedex, France

²LNE-SYRTE, UMR8630, Observatoire de Paris, 61 avenue de l'Observatoire, 75014 Paris, France

³Office National d'Etude et de Recherches Aérospatiales, Chemin de la Hunière, 91761 Palaiseau, France

ABSTRACT

We present our the construction of an atom interferometer for inertial sensing in microgravity, as part of the I.C.E. (*Interférométrie Cohérente pour l'Espace*) collaboration. On-board laser systems have been developed based on fibre-optic components, which are insensitive to mechanical vibrations and acoustic noise, have sub-MHz linewidth, and remain frequency stabilised for weeks at a time. A compact, transportable vacuum system has been built, and used for laser cooling and magneto-optical trapping. We will use a mixture of quantum degenerate gases, bosonic ⁸⁷Rb and fermionic ⁴⁰K, in order to find the optimal conditions for precision and sensitivity of inertial measurements. Microgravity will be realised in parabolic flights lasting up to 20s in an Airbus.

1. INTRODUCTION

Intense research effort has focussed on the study of degenerate quantum gases and macroscopic matter waves since their first observation in 1995. Atom interferometers benefit from the use of trapped ultracold atomic gases, gaining good signal-to-noise ratios due to the high atomic densities, and the coherence required for the visibility of interference patterns due to the low temperatures[1]. The sensitivity of an interferometric measurement also depends on the interrogation time, the time during which the sample freely evolves. This time is limited by both the free-fall of the atomic cloud, requiring tall vacuum chambers, and by its free expansion, demanding extra-sensitive detection systems for extremely dilute clouds. Ultralow temperatures further reduce the expansion.

In conceiving the next generation of extreme-precision atom interferometers, there is much to be gained by performing experiments in microgravity [2, 3]. Free-fall heights of more than 100m, corresponding to durations of 5 seconds or more are available either in a drop tower (e.g. ZARM Bremen, Germany) or in a parabolic flight

in an aeroplane. Laboratory experiments are limited to about 300ms of free fall. The sensitivity of an interferometric accelerometer increases quadratically with time, and thus one can expect to gain more than two orders of magnitude in having a transportable, drop-compatible device.

There remain questions over the best method to perform atom interferometry. Bosons suffer from interaction shifts leading to systematic errors such as the clock shift, a problem not apparent in ultracold fermions[4]. However, degenerate fermions have an intrinsically broad momentum distribution due to Pauli blocking, limiting the visibility of interference patterns. Furthermore, to achieve quantum degeneracy, fermions must be cooled using a buffer gas, typically an ultracold gas of bosons, thus complicating experiments using fermions. Pairs of fermions (molecules or Cooper pairs[5]) can be created by applying a homogeneous magnetic field (Feshbach resonances[6]), offering yet more possible candidate species for atom interferometers.

A further bonus to free-fall is the possibility of using weaker confining forces for the atoms, since gravity need not be compensated with additional levitation forces[7]. Temperatures achieved by evaporative cooling and adiabatic expansion are lowered as the trapping potential is reduced. Not only does the sensitivity of an interferometric measurement benefit, but also new phases of matter may be observed if the kinetic energy can be made smaller than the interatomic potential. A reduced-gravity environment will permit study of new physical phenomena, e.g. spin dynamics and magnetic ordering (see for example [8] and references therein).

This article presents our design for a transportable, boson-fermion mixture, atom interferometer, compatible with a parabolic flight in an aeroplane.

1.1. Overview of the Experiment

The central components of this project are the atomic-physics vacuum system, the optics, and their supports. The atomic manipulation starts with alkali-metal vapour dispensers for rubidium and potassium[9]. A slow jet of atoms is sent from the collection chamber by a dual-species, two-dimensional, magneto-optical trap (2D-MOT) to the trapping chamber, for collection and cooling in a 3D-MOT. Atoms are then be transferred to a conservative, far-off-resonance optical-dipole trap (FORT) for further cooling towards degeneracy. The sample is then ready for coherent manipulation in an atom-interferometer. Raman two-photon transition will be used as atomic beam-splitters and mirrors. Three-pulse sequences ($\pi/2 - \pi - \pi/2$) will be used for accelerometry.

All light for the experiment arrives by optical fibres, making the laser sources independent of the vacuum system. Transportable fibred laser sources for laser cooling and trapping have been fabricated with the required frequency stability. The techniques for mechanically-stable power distribution by free-space fibre couplers function according to specifications. The vacuum chamber is compatible with the constraints of microgravity in an Airbus parabolic flight. Such a flight permits total interrogation times up to 7s, giving a potential sensitivity of better than 10^{-9} m s^{-2} per shot, limited by phase noise on the frequency reference for the Raman transitions.

2. LASER SYSTEMS

2.1. Continuous-Wave Fibre-Laser Source at 780 nm for Rubidium Cooling

An entirely pigtailed laser source is particularly appropriate in our case as it does not suffer from misalignments due to environmental vibrations. Moreover, telecommunications laser sources in the C-band (1530–1570 nm) have narrow linewidths ranging from less than 1MHz for laser diodes, down to a few kHz for Erbium doped fibre lasers. By second-harmonic generation (SHG) in a nonlinear crystal, these $1.56\mu\text{m}$ sources can be converted to 780nm sources [10, 11, 12]. Such devices avoid having to use extended cavities as their linewidths are sufficiently narrow to satisfy the requirements of laser cooling.

Our laser setup is sketched in Figure 1. A 1560nm Erbium doped fibre laser is amplified by a 500mW polarisation-maintaining (PM) Erbium-doped fibre amplifier (EDFA). A 90/10 PM fibre-coupler directs 10% of the pump power to a pigtailed output. 90% of light is then sent into a periodically-poled Lithium-Niobate Waveguide (PPLN-WG). This crystal is pigtailed on both sides with 1560nm single-mode fibres. The input fibre is installed in a polarisation loop system in order to align the

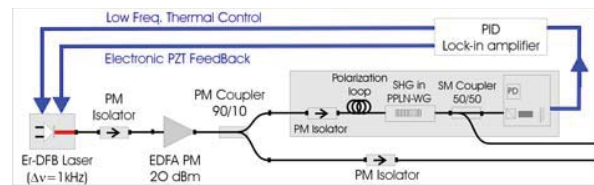


Figure 1. Transportable laser set-up schematic. A double-loop feedback system is used for frequency control: the first returns a saturated absorption signal to the piezoelectric transducer; the second loop compensates thermal drifts of the fibre laser when the error signal of the first loop becomes large.

electric field with principal axes of the crystal. A fibre-coupler which is monomode at 780nm, filters pump light after the crystal and sends half of the 780nm light into a saturated-absorption spectroscopy device for frequency servo-control. The other half is the frequency-stabilised pigtailed output. The whole device, including the frequency control electronics was implemented in a rack for ease of transport. Typical output from the first generation device was $500\mu\text{W}$ of 780nm light, with more than 86dB attenuation of 1560nm light after 3m of monomode fibre. A more recent version ($> 50\text{mW}$) has been used to power a magneto-optical trap.

Two PPLN-WGs from HC-Photonics were tested. Both have a poling period appropriate for SHG at 780nm. They have the same quasi-phase matching temperature of 63°C . The first is 13mm long, doped with 1% MgO, and is used in our laser source. The second is 30mm long, doped with 5% MgO. Figure 2 gives the output power as a function of the pump power. The 13mm long crystal has a fibre-to-fibre efficiency of 10%/W. The fit curve corresponds to the non-depleted pump regime. Photorefractive effects appear around 10mW of 780nm light. In practice the laser is run with 100mW pump power. Power fluctuations in this crystal are due to two phenomenon: first the input fibre does not maintain polarisation, and polarisation fluctuations lead to a variation of the output power. Secondly the output fibre of the crystal is not single mode at 780nm. Thus the power distribution in the fundamental mode varies with time, leading to power fluctuations when the crystal is pigtailed to a single-mode fibre at 780nm. The second crystal has a fibre-to-fibre efficiency of 120%/W for low pump power. The fit curve corresponds to a depleted regime. Photorefractive threshold is estimated around 60mW of second harmonic. The input fibre is still not polarisation maintaining, leading to output power drifts, but the output fibre is PM and single mode at 780nm, which greatly reduces power fluctuations.

2.2. Fibre Power Splitters

The optical bench and the vacuum chamber are not rigidly connected to each other, and laser light is transported to the vacuum chamber using optical fibres. Sta-

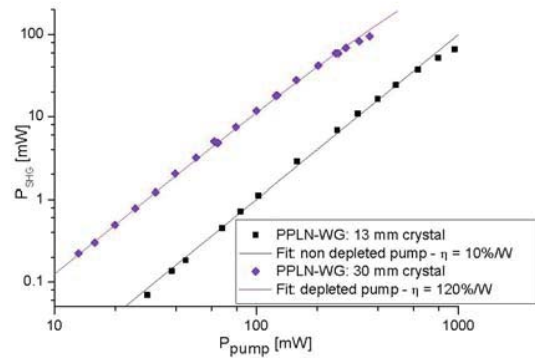


Figure 2. Second-harmonic generation as a function of pump power. Two crystals (13mm, 30mm) were tested. Fits to non-depleted pump (13mm crystal, 10%/W efficiency, squares) and depleted pump (30mm crystal, 120%/W, lozenges).

bility in trapping and coherent atom manipulation is assured by using only polarisation maintaining fibres. Six trapping and cooling laser beams are needed for the 3D-MOT and five for the 2D-MOT, with relative power stability better than a few percent. We have developed fibre beam-splitters based on polarising cubes and half-wave plates with one input fibre and the relevant number of output fibres. The stability of the beam splitters has been tested by measuring the ratio of output powers between different outputs as a function of time. Fluctuations are negligible on short time scales (less than 10^{-4} relative intensity over 1s), and very small over typical periods of experimental operation (less than 1% over a day). Even over months, drifts in power distribution are only a few percent, which is sufficient for this experiment.

3. MECHANICAL AND VACUUM SYSTEMS

The mechanical construction of the apparatus is critical to any free-fall experiment. Atomic-physics experiments require heavy vacuum systems and carefully aligned optics. Our design is based around a cuboidal frame of foam-damped hollow bars with one face being a vibration-damped optical breadboard: see Figs. 3 and 4. The outside dimensions are $1.2\text{m} \times 0.9\text{m} \times 0.9\text{m}$, and the total weight of the final system is estimated to be 400kg (excluding power supplies, lasers, control electronics, air and water flow). The frame provides support for the vacuum system and optics, which are positioned independently of one another. The heavy parts of the vacuum system are rigged to the frame using steel chains and high-performance polymer slings under tension, adjusted using turnbuckles; most of the equipment being standard in recreational sailing or climbing. The hollow bars have precisely positioned grooves which permit optical elements to be rigidly fixed (bolted and glued) almost

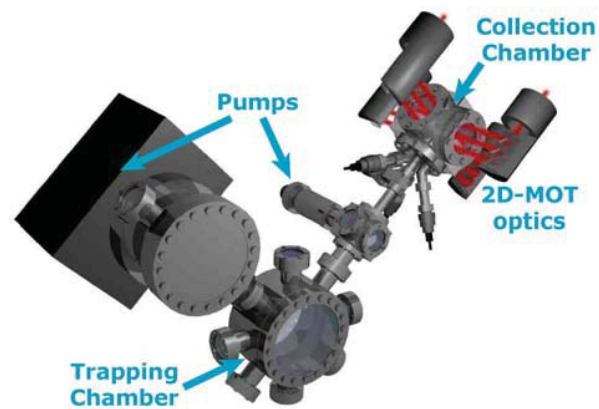


Figure 3. Artist's impression of the vacuum system. Atoms are transferred from the collection chamber, using a 2D-MOT, to the trapping chamber, where they are collected in a 3D-MOT. The trapping chamber has large optical accesses for the 3D-MOT, optical-dipole trap (FORT), imaging, and interferometry. There is a getter pump between the two chambers to ensure a large pressure difference. The other pump is a combined ion pump-titanium sublimation pump.

anywhere in the volume within the frame. An adaptation for transportability will be to enclose the frame in a box, including acoustic and magnetic shielding, temperature control, air overpressure (dust exclusion), as well as ensuring safety in the presence of the high-power lasers.

The vacuum chamber has three main parts: the collection chamber (for the 2D-MOT), the trapping chamber (for the 3D-MOT and the FORT) and the pumps (combined ion pump and titanium sublimation pump). Between the collection and trapping chambers there is an orifice and a getter pump, allowing for a high differential pressure, permitting rapid collection by the 2D-MOT but low trap losses in the 3D-MOT and FORT. The magnetic coils for the 2D-MOT are under vacuum, and consume just 5W of electrical power.

The main chamber has two very large viewports as well as seven side windows (and one entry for the atoms from the 2D-MOT). Thus there is plenty of optical access for the 3D-MOT, the FORT, imaging and interferometry. To preserve this optical access, the magnetic coils are outside of the chamber, although this markedly increases their weight and power consumption.

To avoid heating due to vibrations in the FORT optics, or measurement uncertainties due to vibrations of the imaging system, the trapping chamber is as close to the breadboard as possible. For laboratory tests, the breadboard is lowest, and the 2D-MOT arrives at 45° to the vertical, leaving the vertical axis available for addition of interferometry for precise measurements, e.g a standing light wave. Around the main chamber, large electromagnet coils in Helmholtz-configuration will be added, to produce homogeneous, stable fields up to 0.12T (1200G), or

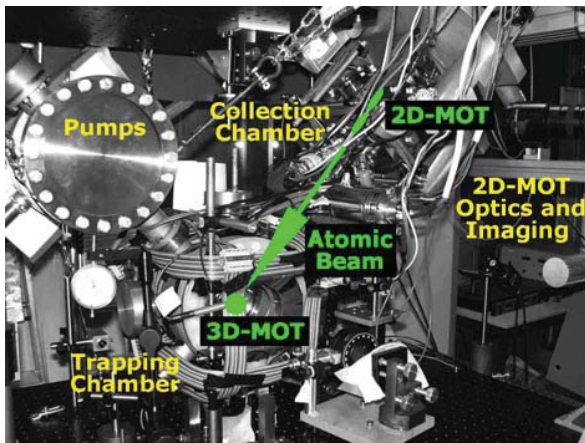


Figure 4. Photograph of the vacuum chamber, the support structure and the optics for magneto-optical traps.

gradients up to 0.6T/m (60G/cm).

3.1. 2D-MOT

The 2D-MOT is becoming a common source of cold-atoms in two-chamber atomic-physics experiments[13], and is particularly efficient for mixtures [14] of ^{40}K and ^{87}Rb , if isotopically enriched dispensers are used. Briefly, a 2D-MOT has four sets of beams (two mutually orthogonal, counter-propagating pairs) transverse to the axis of the output jet of atoms, and a cylindrical-quadrupole magnetic field generated by elongated electromagnet pairs (one pair, or two orthogonal pairs). Atoms are cooled transverse to the axis, as well as collimated. Implicitly, only slow atoms spend enough time in the 2D-MOT to be collimated, so the output jet is longitudinally slow. The number of atoms in the jet can be increased by the addition of the push beam, running parallel to the jet: a 2D-MOT⁺. Typically the output jet has a mean velocity below 30m s^{-1} , with up to 10^{10} at s^{-1} of ^{87}Rb and 10^8 at s^{-1} of ^{40}K .

Our design uses 40mW per species for each of the four transverse beams, each divided into two zones of about 20mm using non-polarising beam-splitter cubes, corresponding to about three times the saturation intensity for the trapping transitions. The push beam uses 10mW of power, and is about 6mm in diameter. Each beam comes from an individual polarisation-maintaining optical fibre, with the light at 766.5nm and 780nm being superimposed on entry to the fibres. The 2D-MOT is seen as two bright lines of fluorescence in the collection chamber.

3.2. 3D-MOT and Optical-Dipole Trap

The atomic jet from the 2D-MOT is captured by the 3D-MOT in the trapping chamber. At the time of writing, we

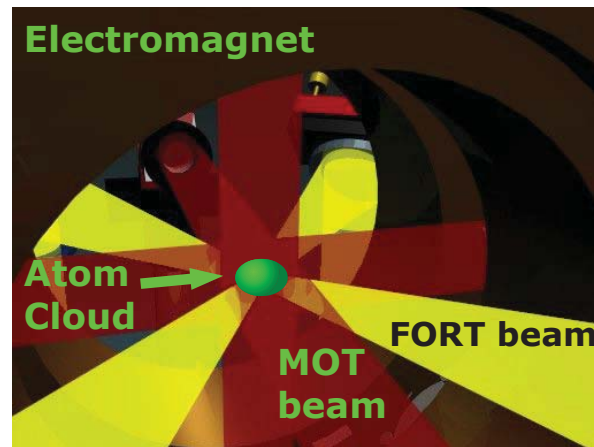


Figure 5. Artists impression of the 3D-MOT (dark, red beams, and the electromagnets) and Far-Off-Resonance Optical-Dipole Trap (pale, yellow beams).

have observed the transfer and capture of atoms, significantly increased by the addition of the push beam[15]. The 3D-MOT uses one polarisation-maintaining fibre input per species. Beams are superimposed and split into 6 arms (on a small optical breadboard fixed near one face of the frame) for the three, orthogonal, counter-propagating beam pairs. Once enough number of atoms are collected in the 3D-MOT, the 2D-MOT is to be turned off, and the 3D-MOT optimised for transfer to the FORT.

The FORT will consist of two, nearly-orthogonal (70°) beams making a crossed, dipole trap using 50W of light at 1565nm. We will have rapid control over intensity using an electro-optical modulator, and beam size using a mechanical zoom, after the design of Kinoshita et al.[16]. Optimisation of transfer from the 3D-MOT to the FORT, and the subsequent evaporative cooling will require experiments. Strong, homogeneous, magnetic fields will be used to control interspecies interactions via Feshbach resonances[6], to expedite sympathetic cooling of ^{40}K by ^{87}Rb .

We can expect to load the 3D-MOT during less than 5s, then cool to degeneracy in the optical-dipole trap in around 3–10s. Thus we will be able to prepare a sample for interferometry in less than the free-fall time of a parabolic flight (around 20s).

4. CONCLUSIONS

We have shown our design for a transportable atom interferometer for parabolic flights in an Airbus. The device is built in two main parts, the laser systems and the atomic physics chamber. We have made major technical advances: high-stability frequency synthesis for coherent atom manipulation, flight-compatible laser sources and fibre power splitters, as well as a rugged atomic-physics chamber.

The I.C.E. collaboration is funded by the CNES, as is RAN's fellowship. Further support comes from the European Union STREP consortium FINAQS.

REFERENCES

- [1] Atom Interferometry, edited by P. R. Berman (Academic Press, Boston, 1997).
- [2] T Sleator, PR Berman, B Dubetsky, arXiv:physics/9905047 (1999)
- [3] K Bongs and K Sengstock, *Rep. Prog. Phys.* **67** 907–963 (2004).
- [4] S Gupta, Z Hadzibabic, MW Zwierlein, CA Stan, K Dieckmann, CH Schunck, EGM van Kempen, BJ Verhaar, W Ketterle, *Science* **300** 1723–1726 (2003) and MW Zwierlein, Z Hadzibabic, S Gupta, W Ketterle, *Phys Rev Lett* **91** 250404 (2004)
- [5] CA Regal, M Greiner, DS Jin, *Phys. Rev. Lett.* **92**, 040403 (2004)
- [6] G. Ferrari, M. Inguscio, W. Jastrzebski, G. Modugno and G. Roati, *Phys. Rev. Lett.*, **89** 053202 (2002) and F. Ferlaino, C. D'Errico, G. Roati, M. Zaccanti, M. Inguscio, and G. Modugno, arXiv:cond-mat/0510630 (2005)
- [7] A. E. Leanhardt, T. A. Pasquini, M. Saba, A. Schirotzek, Y. Shin, D. Kielpinski, D. E. Pritchard, W. Ketterle, *Science* **301**, 1513-1515, (2003).
- [8] H. Schmaljohann, M. Erhard, J. Kronjger, K. Sengstock, K. Bongs, *Appl. Phys. B* **79** 1001–1007 (2004).
- [9] Natural-abundance dispensers are available from SAES Getters . We are interested in the isotopes ^{87}Rb and ^{40}K , which are respectively 28% and 0.012% naturally abundant. We will be investing in isotopically enriched ^{40}K (about 5%) dispensers in the near future.
- [10] V Mahal, A Arie, MA Arbore, MM Fejer, *Opt. Lett.* **21**, 1217 (1996)
- [11] RJ Thompson, M Tu, DC Aveline, N Lundblad, L Maleki, *Opt. Exp.* **11**, 1709 (2003)
- [12] J Dingjan, B Darquié, J Beugnon, MPA Jones, S Bergamini, G Messin, A Browaeys, P Grangier, *App. Phys. B* **82**, 47 (2006)
- [13] K Dieckmann, RJC Spreeuw, M Wiedemüller and JTM Walraven, *Phys. Rev. A*, **58** p3891 (1998)
- [14] C. Ospelkaus, S. Ospelkaus, K. Sengstock and K. Bongs, *Phy. Rev. Lett.*, **96** 020401 (2006)
- [15] Our current best measurements are rather vague, suggest $> 5 \times 10^7$ atoms in the cloud. However, the maximum size may in fact be several 10^9 atoms. Loading to nearly the maximum atom number takes less than 5s.
- [16] T. Kinoshita, T.R. Wenger and D.S. Weiss, *Phys. Rev. A*, **71** 01162(R) (2005)